Ethanol-Perturbed Amyloidogenic Self-Assembly of Insulin: Looking for Origins of Amyloid Strains†

Wojciech Dzwolak,*,‡ Stefan Grudzielanek,§ Vytautas Smirnovas,‡,§,|| Revanur Ravindra,§ Chiara Nicolini,§ Ralf Jansen,§ Anna Loksztejn,‡ Sylwester Porowski,‡ and Roland Winter*,§

Institute of High Pressure Physics, Polish Academy of Sciences, Sokolowska 29/37, 01-142 Warsaw, Poland, and Physical Chemistry I-Biophysical Chemistry, Department of Chemistry, University of Dortmund, Otto-Hahn Strasse 6, D-44227 Dortmund, Germany

Received February 15, 2005; Revised Manuscript Received May 3, 2005

ABSTRACT: A model cosolvent, ethanol, has profound and diversified effects on the amyloidogenic self-assembly of insulin, yielding spectroscopically and morphologically distinguishable forms of β-aggregates. The alcohol reduces hydrodynamic radii of insulin molecules, decreases enthalpic costs associated with aggregation-prone intermediate states, and accelerates the aggregation itself. Increasing the concentration of the cosolvent promotes curved, amorphous, and finally donut-shaped forms. According to FT-IR data, inter-β-strand hydrogen bonding is stronger in fibrils formed in the presence of ethanol. Mechanisms underlying the polymorphism of insulin aggregates were investigated by spectroscopic (CD, FT-IR, and fluorescence anisotropy) and calorimetric (DSC and PPC) methods. The nonmonotonic character of the influence of ethanol on insulin aggregation suggests that both preferential exclusion (predominant at the low concentrations) and direct alcohol−protein interactions are involved. The perturbed hydration of aggregation nuclei appears to be a decisive factor in selection of a dominant mode of β-strand alignment. It may override unfavorable structural consequences of an alternative strand-to-strand stacking, such as strained hydrogen bonding. A hypothetical mechanism of inducing different amyloid "strains" has been put forward. The cooperative character of fibril assembly creates enormous energy barriers for any interstrain transition, which renders the energy landscape comblike-shaped.

Aggregation and amyloidogenesis, the common fate of destabilized protein molecules, were implicated in the etiology of several diseases, which has become the main rationale for studies in this field (*1*). Many proteins even with a marginal sequential propensity to form the β-sheet fold (*2*) may be converted to amyloid (a linearly ordered aggregate) under destabilizing pH conditions (*3*−*6*). The case of natively unfolded proteins, such as α-synuclein, proves that a disordered conformation must yet encounter favorable physicochemical circumstances to become susceptible to aggregation (*7*, *8*). The hydrophobicity of many amyloidogenic proteins (e.g., A-β peptide) indicates that protein hydration plays a role in triggering "conformational diseases". Transitions from an unfolded state to either a native conformation (folding) or amyloid (aggregation) may be conceptualized as two competing strategies for minimizing frustration stemming from dangling hydrogen bonds (*9*). Protein ASA[1] and solvent exposure of hydrophobic residues, and a solvophobic backbone (*10*), could be taken as criteria of thermodynamic frustration of protein−water interactions (*11*). Therefore, the hierarchical assembly of amyloids reflects an alternative to the native packing conformational struggle of a polypeptide chain to reduce its ASA and saturate hydrogen bonding, while a simultaneous decrease in the configurational entropy of the protein is offset by gains in solvent entropy. The observed coincidence of amyloid-related illnesses with the patients' age suggests that some extra- and intracellular factors, such as natural osmolytes, may escape mechanisms of physiological regulation at an old age, and play a role in triggering the disease. Glycerol and trimethylamine *N*-oxide (TMAO), which normally rectify folding defects in proteins, are capable of inducing aggregation of Alzheimer β-peptide (*12*). The role of hydrational forces in protein aggregation in vivo, while still poorly understood, may be instrumental in elucidating the molecular basis of amyloidosis and, as such, attracts considerable interest (*13*).

Under physiological conditions, insulin forms hexamers coordinating two or four Zn^{2+} ions. Decreasing the pH and protein concentration shifts the equilibrium toward smaller oligomers. At pH 2, insulin forms dimers in water and

† W.D. acknowledges financial support from the Polish State Committee for Scientific Research, Grant 2P04A 011 28 (2005-2007). R.W. acknowledges financial support from the Deutsche Forschungsgemeinschaft (DFG-FOR 436). W.D. and R.W. also acknowledge support from the COST D30 action "High Pressure Tuning of Biochemical Processes: Protein Dynamics and Aggregation".

* To whom correspondence should be addressed. W.D.: phone, +48 22 888 0237; fax, +48 22 632 4218; e-mail, wdzwolak@unipress.waw.pl. R.W.: phone, +49 231 755 3900; fax, +49 231 755 3901; e-mail, winter@pci.chemie.uni-dortmund.de.

‡ Polish Academy of Sciences.

§ University of Dortmund.

|| Present address.

[1] Abbreviations: AFM, atomic force microscopy; ANS, 1-anilinonaphthalene-8-sulfonic acid; ASA, accessible surface area; CD, circular dichroism; DSC, differential scanning calorimetry; FT-IR, Fourier-transform infrared; HAc, acetic acid; PPC, pressure perturbation calorimetry; TFE, trifluoroethanol; ThT, thioflavin T.

10.1021/bi050281t CCC: $30.25
Published on Web 05/28/2005

monomers in 20 wt % acetic acid (*14*) or ethanol (*15*, *16*). Aggregation of insulin is enhanced under conditions promoting destabilized monomers and dimers, such as low pH, high temperatures, and hydrophobic media. A non-native monomer is likely to be the aggregation-competent intermediate state of the protein (*4*, *5*, *17*). The multistage character of the insulin aggregation has been captured by DSC, which resolved an endothermic formation of the intermediate, followed by an exothermic stacking of protein particles, reduction in protein−water contacts, and precipitation (*18*). The process is energetically self-sustaining, which enables induction of amyloid through seeding with preformed fibrils. Infrared spectra of insulin amyloid suggest a parallel arrangement of the β-strands (*19*), which agrees with a three-dimensional model of the fibrils (*20*). Morphological studies on the insulin amyloidogenesis stress hierarchical intertwining of protofilaments (*21*). Our AFM studies produced evidence for structural polymorphism of insulin fibrils, represented by the circular amyloid formed under high pressure (*22*), and the morphological variety within "ambient" samples (*23*). Insulin fibrils with distinct infrared features and morphologies are obtained in the presence of cosolvents (*24*, *25*). Likewise, morphologies of fibrils obtained in vitro from the Alzheimer's β-peptide are dependent of the presence of a cosolvent at the aggregation stage (*26*). In our earlier studies, we have reported intriguing seeding properties of two types of insulin fibrils grown in water or in an ethanol solution (*27*, *28*). When cross-seeded, the fibrils reproduce their own folding patterns regardless of environmental factors favoring alternative fibrillar types. The two distinct, self-propagating conformational templates mimic the fundamental aspects of the phenomenon of "prion strains" (*29*), implying that strains may reflect a common generic trait of amyloids.

As understanding of solvational control of the aggregation pathways can be a key to untangling molecular mechanisms of amyloid-related diseases, it has motivated this study on the model insulin−ethanol system. We are showing that the hydrational state of the protein in the nucleation phase of aggregation has profound consequences for its self-assembling pattern and may be among decisive factors determining physicochemical and biological properties of the mature amyloid.

PPC is a novel approach (*30*) enabling precise measurements of the apparent thermal expansion coefficient, α_P, as a function of temperature. α_P-T curves of a dissolved protein reflect the kosmotropic (mostly hydrophobic) or chaotropic (polar and charged) character of amino acid side chain residues interacting with the surrounding solvent. Dramatic changes in α_P-T plots during thermal denaturation arise from water structuring properties of amino acids exposed to the bulk solvent upon unfolding different from those for amino acids interacting with the solvent in the native state (*30*−*33*). For PPC, the calorimeter was equipped with MicroCal's PPC accessory. The physical principles and detailed methodology are described elsewhere (*30*).

MATERIALS AND METHODS

CD

Concentrations of bovine insulin (from Sigma) in 0.1 M NaCl (pH 1.9) were 0.5 and 0.8 mg/mL for the far- and near-UV CD, respectively. Spectra were recorded on a JASCO J-715 spectropolarimeter in cylindrical cells (1 and 10 mm path lengths for the far-UV and near-UV CD, respectively). The temperature was increased from 10 to 70 °C at a rate of 20 °C/h.

FT-IR

Insulin (2 wt %) in 0.1 M NaCl and D_2O (pD 1.9, uncorrected) was incubated for 1 h at 10 °C to complete the H−D exchange of unprotected protons. For studying the ethanol concentration effect, samples were prepared in the same regimes as for AFM. The temperature in the cell was increased from 10 to 60 °C at a rate of 20 °C/h. Spectra were collected on a Nicolet NEXUS FT-IR spectrometer. For each spectrum, 256 interferograms of 2 cm^{-1} resolution were co-added. For data processing, GRAMS (Thermo-Nicolet) was used.

Fluorescence Spectroscopy

ThT Assay. Insulin (0.5 wt %) and ThT were dissolved in 0.1 M NaCl (pH 1.9) at a final protein:dye molar ratio of 50:1. Samples were continuously stirred during measurements at 50 °C [$\lambda_{ex} = 450$ nm, $\lambda_{em} = 482$ nm (*36*)].

Labeling with Alexa 488. Labeling with Alexa 488 succinimidyl ester (Molecular Probes) was carried out in 685 μM insulin, at pH 8.3, with a 2:1 protein:fluorophore molar ratio (*6*, *34*). Final samples contained 0.5 wt % insulin at a protein:dye ratio of 1000:1 in 0.1 M NaCl (pH 1.9).

Fluorescence Measurements. Fluorescence anisotropy measurements of the Alexa-labeled samples were performed on an ISS K2 fluorometer ($\lambda_{ex} = 490$ nm, $\lambda_{em} = 520$ nm), at a heating rate of 20 °C/h. Anisotropy was calculated as described elsewhere (*35*). The data were analyzed in terms of Perrin plots employing the Stokes−Einstein equation for isotropic unhindered rotation of a sphere:

$$\frac{1}{r} = \frac{1}{r_0} + \frac{R\tau}{r_0 V_h}\frac{T}{\eta} \quad (1)$$

where r is the anisotropy, r_0 the limiting anisotropy, 0.375 for Alexa 488 (*36*), R the gas constant, T the temperature, η the solvent viscosity, τ the average fluorescence lifetime, and V_h the hydrodynamic volume of the rotating particle. The plot of $1/r$ versus T/η yields a straight line if fluorescing units behaves like rotating spheres. Values for η are from the literature (*37*). Assuming a common r_0, and τ unaffected by the solvent composition, the $V_{h,1}/V_{h,2}$ ratio (reflecting the protein association state) is approximated by an inverted ratio of the respective Perrin plot slopes. For calculating absolute hydrodynamic volumes, time-resolved measurements were performed at various temperatures (5−35 °C), with the modulation of the fluorescence lifetime by varying solvent compositions taken into account (*35*). The lifetime data were analyzed with Globals Unlimited software.

ThT and ANS Titration of Amyloid Samples

Samples obtained through incubation of 17.3 μM insulin for 96 h at 50 °C and pH 1.9 in different cosolvents at a concentration of 20 wt % were assayed for dye binding by centrifugation and resuspension in 20 μM ANS, or 50 μM ThT in 0.1 M aqueous NaCl. Binding was assessed by UV

absorbance measurements (at 412 nm for ThT and 350 nm for ANS) of supernatants (A_s) after the dye capture by amyloid. The fraction of bound fluorophores, f_b, was calculated with the relationship $f_b = 1 - (A_s/A_t)$, where A_t is the absorbance of 20 μM ANS or 50 μM ThT.

DSC and PPC

For DSC and PPC, 2 wt % insulin in 0.1 M NaCl (pH 1.9) at varying concentrations of EtOH was used. DSC was carried out on a VP DSC calorimeter from MicroCal (*18*). The effective scan rate was 20 °C/h. Pressure jumps (5 bar) of N_2 were applied to the samples. Under the same experimental conditions, a set of reference sample−buffer, buffer−buffer, buffer−water, and water−water measurements was carried out each time. The partial molar volume of insulin used for volumetric calculations was 0.71 $cm^3\ g^{-1}$.

AFM

Fresh 0.1 wt %, pH 1.9 insulin solutions were incubated at 60 °C for 24 h. Subsequently, the samples were diluted 400 times with acidified water, and applied onto freshly cleaved muscovite mica. The abrupt dilution of the samples immediately quenches the concentration-dependent aggregation process. Fast drying follows the deposition of tiny droplets on the mica surface, which prevents further aggregation. All AFM images were recorded in the Tapping-in-Air mode on a MultiMode SPM microscope equipped with a Nanoscope IIIa Controller (Digital Instruments). Other methodological details are the same as in ref *23*.

RESULTS

Figure 1 presents far-UV (A) and near-UV (B) CD spectra of insulin at increasing concentrations of ethanol. The increasingly negative Cotton effect at 208 nm and the simultaneous decay of ellipticity at 222 nm suggest that, while ethanol induces disorder, a substantial helical content is retained (Figure 1A). Temperature (*17*), guanidine hydrochloride (*4*), and urea (*5*) affect far-UV CD spectra of human insulin similarly. Four tyrosine residues (per monomer) constitute the major contribution to the near-UV CD of the folded protein at 275 nm as seen in Figure 1B. The decrease in ellipticity at 275 nm at the increasing ethanol concentration indicates destabilization of the tertiary structure. These changes resemble perturbations induced in the CD of human insulin through destabilizing mutations (*38*). As shown in the semiquantitative plots in Figure 1C, both the secondary and tertiary structures of the protein appear to be influenced mostly by low alcohol concentrations. Dependencies of the $[\theta]_{208}/[\theta]_{222}$ ratio, marking changes in the secondary structure, and of $[\theta]_{275}$ level off, once the alcohol content is 25-30 wt %, which corresponds to a molar fraction of 0.13−0.168.

Because this "critical" concentration puts an end to the rapid conformational changes in insulin, while coinciding with the alcohol content known to dissociate native dimers (*15*, *16*) and induce a conformational variant of insulin amyloid (*27*, *28*), it was interesting to see how it affects the far- and near-UV CD spectra of the aggregation-prone intermediate state. Figure 2 shows CD spectra of insulin in water (A and B) and in 20 wt % EtOH (C and D) collected at temperatures increasing up to 70 °C, namely, when amyloidogenic conformations prevail (*17*). Absolute values

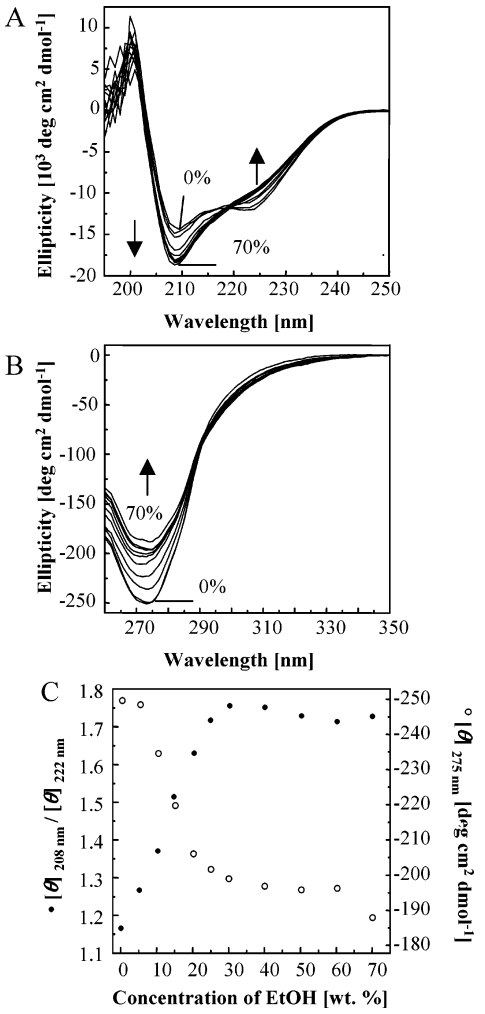

FIGURE 1: Effect of EtOH (weight percent) on far-UV (A) and near-UV (B) CD spectra of insulin in 0.1 M NaCl at pH 1.9 and 20 °C. Quantitative curves illustrate EtOH-induced perturbations of the insulin CD spectra, plotted as a ratio of ellipticity values at 208 and 222 nm (●) and absolute ellipticity values at 275 nm (○) (C).

of ellipticity at 208 and 222 nm decrease simultaneously, indicating that the high-temperature conditions spawn intermediates, which are clearly less helical than the starting conformations. The dramatic decrease in ellipticity at 70 °C (Figure 2A) may be considered to stem from association of molecules, followed by light scattering and partial precipitation of the sample. Such a macroscopic-level effect could remove a portion of the protein molecules from the optical pathway, leading to a marked decrease in the magnitude of the signal. In fact, increasing turbidity may be observed immediately in aggregating aqueous insulin solutions. The lack of such prominent changes in the insulin samples in 20 wt % EtOH (Figure 2C) hints at the relative retardation of the aggregation process under the particular conditions of concentration, temperature, and cosolvent presence. Changes in the near-UV CD spectra (Figure 2B,D) reflect ongoing local rearrangements of the tyrosine residues. The spectra below and at ∼30 °C differ by a markedly more negative ellipticity at 275 nm of the water-dissolved protein (−250 vs −200 deg cm^2 $dmol^{-1}$ for the sample containing EtOH), pointing to a higher degree of order of tyrosine side chains in the former. However, at 60 °C this difference becomes negligible. As the light scattering is likely to obscure an

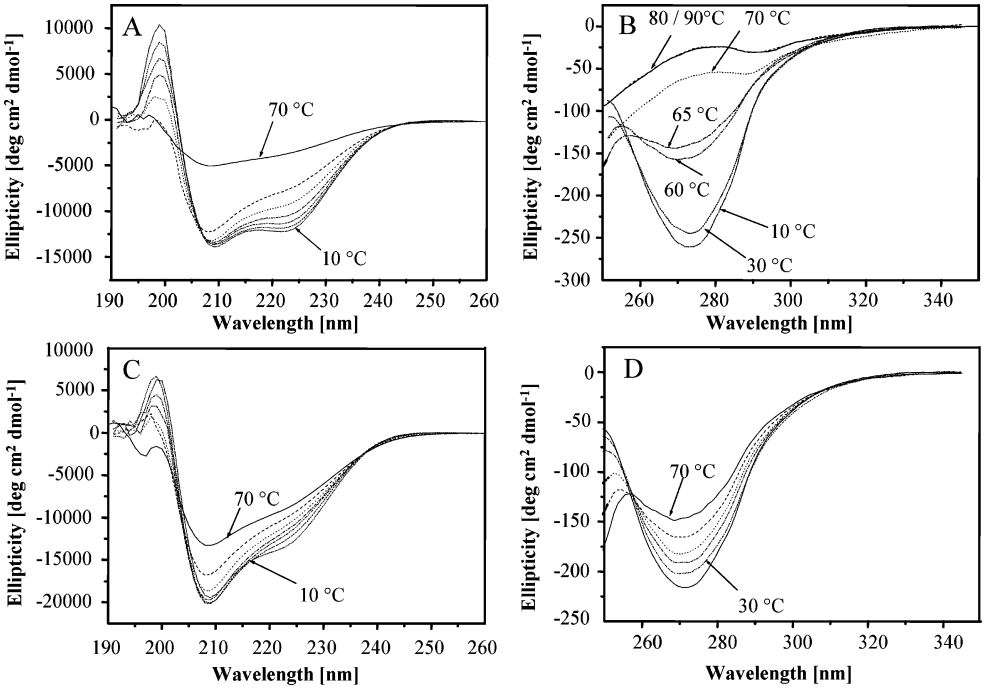

FIGURE 2: Far- and near-UV CD spectra of insulin in 0.1 M NaCl at pH 1.9 (A and B) and in the presence of 20 wt % EtOH (C and D) at increasing temperatures (heating rate of 20 °C/h).

unambiguous analysis of a protein's CD spectra at high temperatures, FT-IR spectroscopy (a method less vulnerable to such artifacts) has been applied for characterization of further stages of insulin fibrillization.

The infrared data confirm that, at the gradually increasing temperature, unfolding occurs before the actual aggregation of insulin aqueous samples (Figure 3A). The decay of the amide II band at 1550 cm^{-1} reflects loosening of the tertiary structure, followed by exposure of protected amide protons to the solvent and H−D exchange, which is greatly enhanced through destabilization of insulin molecules. The progress of H−D exchange has been employed as a yardstick of the protein compactness in the ensuing Figure 3B. A small peak at 1515 cm^{-1} assigned to tyrosine side chains (*39*) remains intact throughout the aggregation, while the secondary structure sensitive amide I band at 1650 cm^{-1} undergoes a profound transition, shifting to 1625 cm^{-1} and narrowing the bandwidth, both of which are hallmarks of the disarray of the native structures and formation of the β-sheet-rich aggregate. A relative intensity plot of the spectral component assigned to the β-sheet delineates the progress of the transition (Figure 3C). Final spectral positions of the amide I′ band depend on the presence (and concentration) of ethanol during the aggregation (Figure 3D). The absorption spectra of D_2O-grown and 20 wt % EtOD-grown amyloids were resolved by the second derivative. The alcohol effect is permanent, and resuspension of once-grown amyloid in an alternative solvent has negligible effects on the absorption maximum. A red shift of the band suggests stronger interstrand hydrogen bonds in the aggregates formed in the presence of ethanol. Similar observations have been reported previously for insulin amyloids grown in the presence of ethanol (*27*, *28*) and acetic acid (*24*, *25*). Because aging of insulin fibrils affects the corresponding infrared spectra, to compare effects of ethanol concentration on the position of the amide I′ band of the amyloid, only uniformly mature amyloid samples obtained after incubation at 60 °C for 24 h were considered (Figure 3E). The data in Figure 3E were obtained for amyloid samples grown in the absence of the salt. This permits a more direct comparison with the corresponding AFM images. As the presence of foreign crystallizing substances in samples for force microscopy damages the quality of the images, the AFM data are typically collected in the absence of salts. According to Figure 3E, the most pronounced effect on the position of the amide I peak of the mature fibrils occurs in the low range of EtOD concentrations (up to ~20 wt %), and levels off at the higher cosolvent ratios.

Although reliable in detecting β-strands and probing hydrogen bonding within them, FT-IR spectroscopy fails to discriminate between amorphous and ordered aggregates. On the other hand, ThT is a selective fluorescent probe emitting strongly when bound to amyloid fibrils, rather than to amorphous aggregates. Therefore, juxtaposing the FT-IR spectra capturing β-aggregation en masse with the amyloid-selective ThT probe is of interest. The influence of ethanol on insulin amyloidogenesis monitored by ThT fluorescence is shown in Figure 4A. The curves feature typical "lag periods", corresponding to the slow formation of nuclei, followed by "elongation phases". Modest concentrations of EtOH (up to ~15 wt %) accelerate both phases. However, in 10 wt % EtOH, the final fluorescence plateau is roughly two-thirds of the "ambient" signal. The higher concentrations lead to a dramatic decrease in fluorescence and retardation of the transition. Since ethanol does not elute ThT from fibrils, and has negligible effects on the fluorescence intensity of ThT intercalated within amyloid fibrils, direct interactions of ThT with EtOH cannot account for the abating fluorescence signal (*7*). Moreover, the plateaus prove that the aggregation is complete, and no free insulin molecules are left in the sample. The data imply that fibrillar aggregates and, by the same token, aggregates capable of binding ThT are formed only at the relatively low ethanol concentration, beyond which amorphous β-pleated fractions dominate.

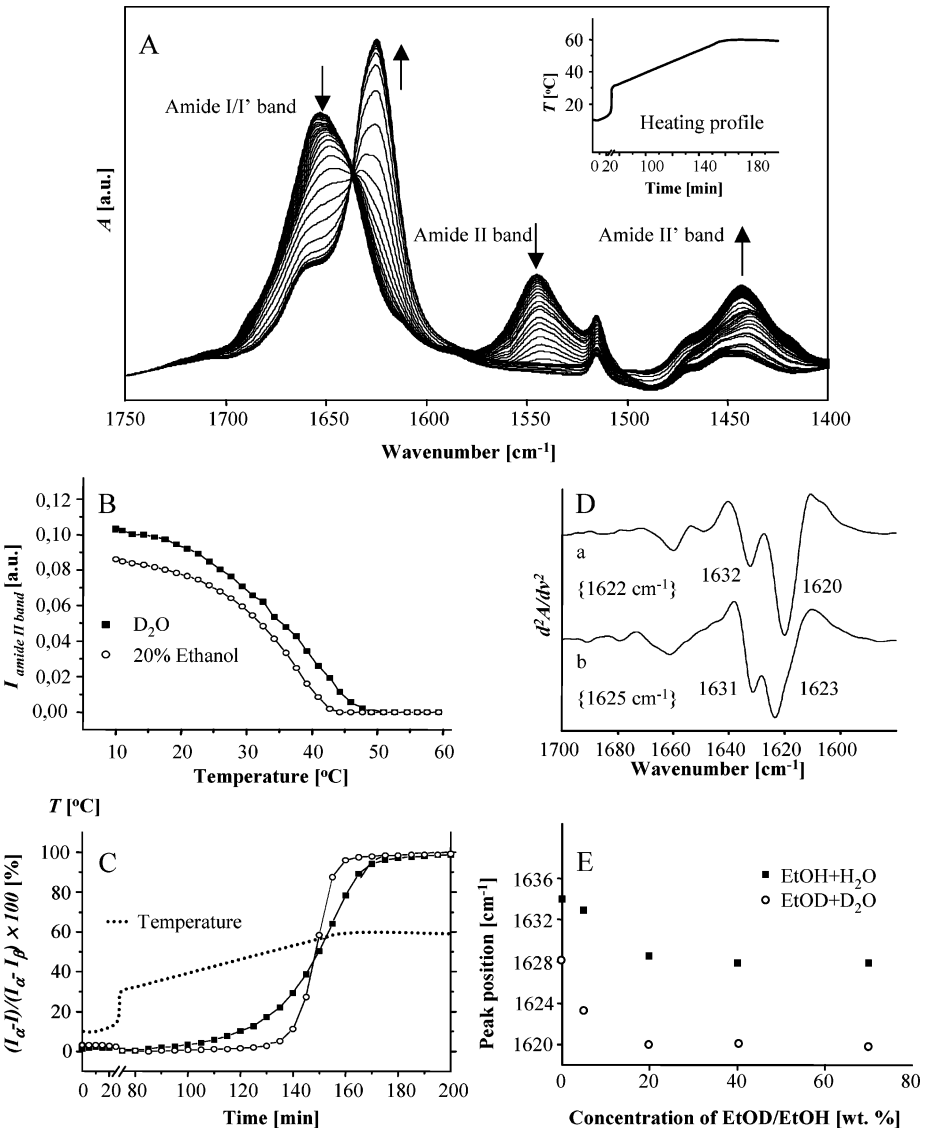

FIGURE 3: (A) Time-resolved FT-IR spectra of 2 wt % insulin in 0.1 M NaCl and D_2O at pD 1.9, gradually heated from 10 to 60 °C at a rate of 20 °C/h, with the heating profile in the inset. (B) A temperature-induced decay of the amide II band precedes the intensity increase of the β-sheet component of the amide I′ band (C). (D) Second-derivative FT-IR spectra after insulin aggregation for 3 h at 60 °C in 0.1 M NaCl and 20 wt % EtOD (a) or in D_2O (b), with the wavenumbers corresponding to the original amide I′ band positions in parentheses. (E) EtOH (and EtOD) concentration effects on the maximum of the amide I′ band of mature amyloid obtained after incubation for 24 h at 60 °C, in the absence of NaCl.

The DSC curve recorded in the absence of ethanol shows an endothermic formation of the intermediate state at 57 °C (*18*), followed by exothermic and irreversible aggregation at 72 °C (Figure 4B). The presence of as little as 5 wt % EtOH causes a striking shift of the exothermic transition to 63 °C, and a simultaneous disappearance of the endothermic peak. The heat released upon insulin aggregation in the presence of ethanol is larger than the corresponding value for water (90 vs 70 kJ/mol). The data in Table 1 demonstrate that the tendency continues with an increasing alcohol content. Certainly, the irreversibility of aggregation rules out taking the "Δ*H*" values for thermodynamically valid figures of enthalpy changes. The transition temperatures follow a less monotonic trend; that is, the lowest temperature of protein aggregation is in 15 wt % ethanol. The further increasing content of alcohol shifts it back to a high-temperature region (Figure 4B and Table 1). This is in accordance with the slower aggregation kinetics at high EtOH concentrations as monitored by ThT fluorescence.

α_P-T dependencies echo chao- or kosmotropic character of chemical groups exposed to the bulk solvent and affecting physicochemical properties, such as the density. Predominantly polar and charged hydrophilic surfaces of native proteins result in positive, decreasing α_P-T plots. Nonpolar and kosmotropic residues, which emerge from a protein's interior only in the event of a major structural destabilization, cause lower α_P values with a tendency to grow with an increase in temperature (*30*). Initially, the α_P-T plot of insulin in water is flat, indicating compensations of the kosmo- and chaotropic surface effects (Figure 5A). Around 50 °C, the intermediate is formed, which, through the exposure of hydrophobic groups, causes an increase in α_P. The area between the experimental points and the baseline (Figure 5A) approximates the volume expansion accompanying the process. The subsequent aggregation is marked with a spike caused by inefficient heat compensation of the robust heat release (*25*). The α_P-T dependence of insulin in 20 wt % ethanol (Figure 5B) features a positive slope, lower α_P

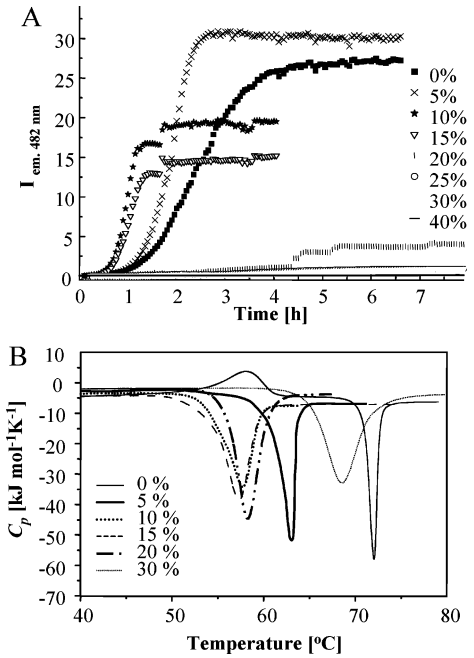

FIGURE 4: (A) Aggregation of 0.5 wt % insulin in 0.1 M NaCl at pH 1.9 and 50 °C probed by the amyloid-bound ThT fluorescence (at the final protein:dye molar ratio of 50:1). (B) Effect of EtOH on DSC scans of insulin.

Table 1: Effect of Ethanol on the Exothermic Phase of Insulin Aggregation

EtOH concentration (wt %)	T_m (°C)	"ΔH" (kJ/mol)
0	72.1	−70
5	63.0	−90
10	57.9	−110
15	57.2	−125
20	58.2	−134
30	68.3	−140

values, and a lack of volume expansion preceding the aggregation. The aggregation is accompanied by a decrease in α_p of ca. 2×10^{-4} K^{-1}, implying the release of protein-bound water and a reduction in the total area of the protein−water interface.

The coincidence of the intermediate transition peaks (the endothermic in Figure 4B and the volume expansion in Figure 5A) with the presence of the dimers (in aqueous samples), but not with monomers (in 20 wt % ethanol), points to a temperature-induced monomerization as a possible underlying mechanism, whose calorimetric (heat uptake) and volumetric (expansion) consequences are detected by DSC and PPC, respectively. Fluorescence anisotropy offers a means of addressing this problem. The Perrin plots corresponding to insulin samples dissolved in water, 5 wt % ethanol, and 20 wt % ethanol are shown in Figure 5C. A ratio of apparent hydrodynamic volumes of molecules may be approximated as an inverse ratio of the corresponding Perrin plot slopes (Materials and Methods), which are $8.08 \pm 0.07 \times 10^{-6}$ Pa s K^{-1} for insulin in water, $1.55 \pm 0.04 \times 10^{-5}$ Pa s K^{-1} in a 5 wt % EtOH solution, and $1.95 \pm 0.02 \times 10^{-5}$ Pa s K^{-1} in a 20 wt % EtOH solution (Figure 5C). Hence, ratios of the apparent hydrodynamic volumes of insulin in the different solvents are as follows: V_h(water):V_h(5 wt % EtOH) = 1.92:1 and V_h(water):V_h(20 wt % EtOH) = 2.41:1. Insulin dimers prevail in water, whereas even 5 wt % EtOH renders the protein predominantly monomeric.

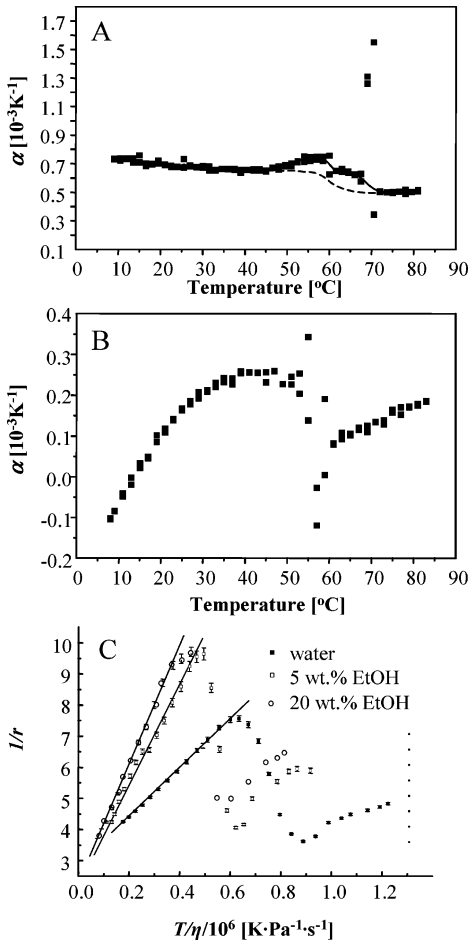

FIGURE 5: PPC plots show the dependence of the partial thermal expansion coefficient of insulin in the absence (A) and presence (B) of 20 wt % EtOH. (C) Perrin plots calculated according to viscosity-corrected temperature dependencies of fluorescence anisotropy of Alexa 488-labeled insulin with and without EtOH.

The line in Figure 5C, denoting dimeric insulin, should bend toward the "monomeric" lines in the event of temperature-induced dissociation. Surprisingly, this is clearly not the case. An abrupt association and aggregation, following immediately dissociation of dimers, can explain the descending of all the three slopes at higher temperatures.

A morphological characterization of the aggregates has been carried out with AFM. Inasmuch as cosolvent-free amyloid species present typical fibrillar features (Figure 6A), the tiny 5 wt % amount of EtOH triggers bends and circular forms, with diameters of typically 750−800 nm (Figure 6B). In 20 wt % ethanol, fibrillar and amorphous aggregates coexist (Figure 6C). When the alcohol concentration is increased further, new, large, donut-shaped bodies appear (Figure 6D−F). A representative specimen of 70 wt % EtOH-grown insulin aggregate (Figure 6F) has a diameter of 700 nm and a height of 315 nm, which is roughly 150 times the height of a single protofilament (*22*). This implies clusters of amorphous aggregates as the most likely products of insulin association at high EtOH concentrations.

As the cosolvent presence triggers conformational variants of β-aggregates of insulin, it was of interest to probe dye binding properties of amyloid samples obtained through a complete aggregation of insulin in the presence of different cosolvents (at a concentration of 20 wt %). Such an approach, while very approximate, gives insight into certain physico-

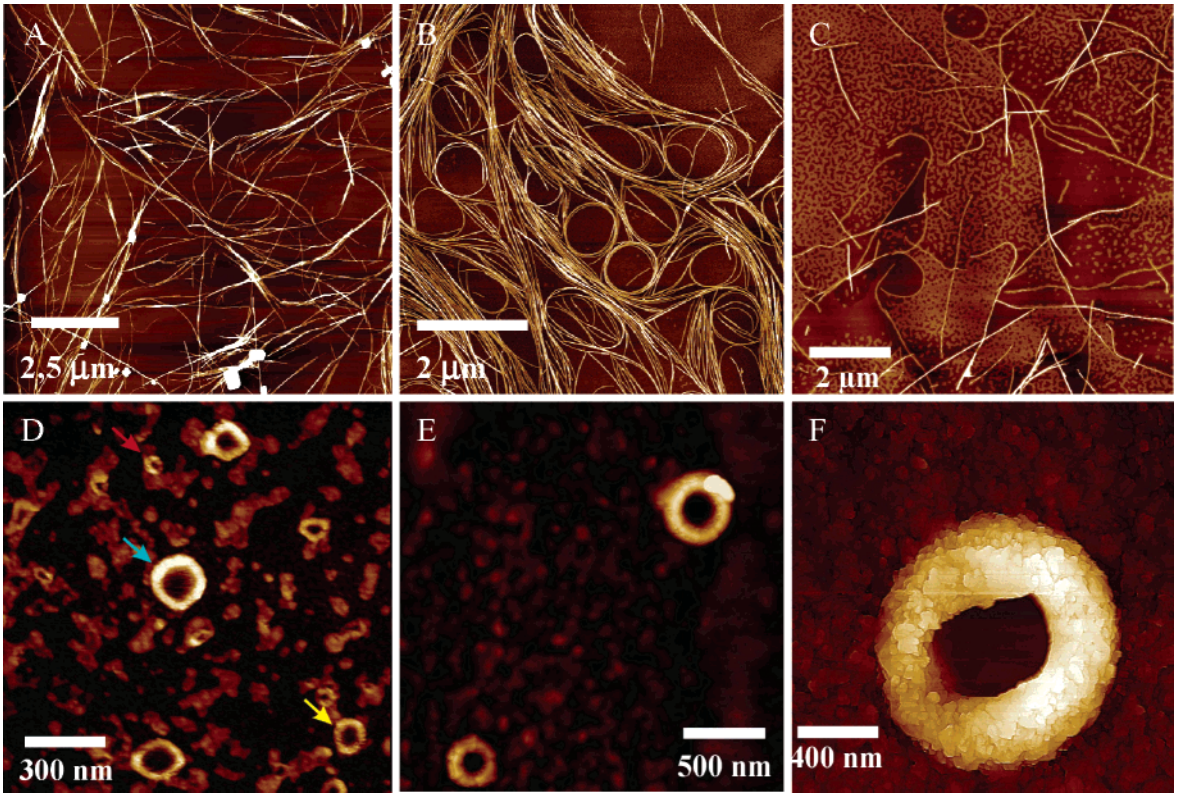

FIGURE 6: AFM height images of insulin aggregates obtained through a 24 h incubation of 0.1 wt % native protein at pH 1.9 and 60 °C in the presence of increasing concentrations of EtOH: 0 (A), 5 (B), 20 (C), 40 (D), and 70 wt % (E and F).

chemical properties of the fibrils, such as surface hydrophobicity, and topological accessibility to dye-binding sites. Two dyes known to interact with exposed hydrophobic residues in partly unfolded protein conformations (ANS) and, on the other hand, mature fibrils (ThT) have been employed for this purpose. The two dyes were used to probe adhesive protein−dye interactions, rather than specific structural properties (manifested in fluorescence). For this reason, UV absorption of amyloid-depleted supernatants was assessed (Materials and Methods). Figure 7 compares the binding of ThT and ANS to that of insulin aggregates formed in the presence of different solvents and cosolvents. Since the effectiveness of the dye capture depends on dispersion of aggregates in solution, comparison of entirely different morphological species [such as straight fibers and the donut-shaped clusters (Figure 6A,F)] is pointless. Instead, dye captures of ordered β-aggregates formed in the presence of different diluted cosolvents at the same concentration were contrasted. Amyloid samples were sequestered from "mother" solutions and quantitatively resuspended in 0.1 M aqueous NaCl. The fibrils formed in pure H_2O, in pure D_2O, or in the presence of glycerol (osmolyte) have lower affinity for both dyes (Figure 7). The presence of ethanol, acetic acid, or TFE fosters growth of fibrils binding ThT and ANS more effectively.

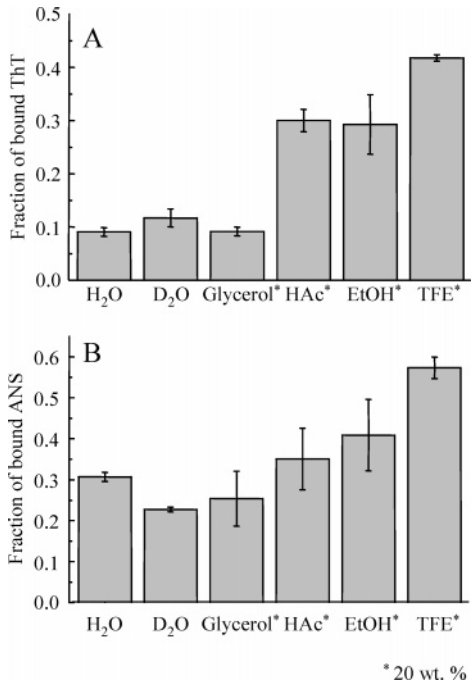

FIGURE 7: Fractions of ThT (A) and ANS (B) captured by insulin amyloid samples prepared in the presence of different cosolvents at a uniform concentration of 20 wt %. Dye binding was assessed by comparative UV absorbance measurements.

DISCUSSION

Insulin has four tyrosine residues, of which Tyr^{A14}, Tyr^{A19}, and Tyr^{B16} reside in helices (*40*). Thus, rather unsurprisingly, along with the far-UV CD spectra, the near-UV CD changes as well (Figure 1C). According to the fluorescence anisotropy (Figure 5C), ethanol dissociates the dimers, which is again expected to influence near-UV CD, as Tyr^{B26} and Tyr^{B16} are directly involved in the stabilization of dimers (*40*). The anisotropy data and the coincidence of the positive DSC and PPC peaks with the presence of dimers provide grounds for claiming that dissociation of dimers underlies the endothermic and volume-expanding process preceding aggregation in aqueous samples. Given that the dissociation occurs at 57 °C (Figure 4B), it is reasonable to expect that at 60 °C,

and in 25-fold diluted samples (DSC vs near-UV CD conditions), monomers prevail. Accordingly, the difference in ellipticity at 30 °C decreases with temperature (Figure 2B,D).

According to the H−D exchange data (Figure 3), solvent exposure of buried amide protons is only slightly enhanced by 20 wt % alcohol. Unlike the DSC, FT-IR does not indicate the pronounced aggregation-accelerating effect of low EtOH concentrations. Apart from D_2O (used in FT-IR but not in DSC), known to prevent aggregation (*18*), different physical principles underlie detection in DSC and FT-IR. Heat capacity changes visible in DSC arise from binding or release of water molecules from protein surfaces. This may occur on time scales shorter than that of the collective rearrangement of hydrogen bonding patterns, which is a prerequisite of stacking β-strands (visible in FT-IR). In fact, clustering of nativelike insulin molecules prior to the aggregation has been proposed (*19*). Should this event take place at a very fast rate (in the presence of EtOH), it obviously hampers the precision of packing of polypeptide chains, which is required for self-assembly of fibrils. In unison with this, the β-aggregates grown at higher ethanol concentrations have progressively disordered morphologies (Figure 6) and declining ThT fluorescence (Figure 4A).

Apart from the kinetic factors, thermodynamic forces are likely to promote the amorphous stacking at the high ethanol concentrations. The hierarchical order of amyloidal self-assembly may be perceived as a collective "struggle" of polypeptide chains to reduce ASA and bury hydrophobic groups. Arguably, the thermodynamic penalty associated with an exposure of hydrophobic groups is strictly coupled to the properties of the environment, such as the local dielectric constant, preferential hydration (mediated by kosmotropes), or preferential binding (to denaturants). While correlations between cosolvent-induced changes in the dielectric constant and the progress of conformational transitions have been reported (*7*, *41*), this approach seems to be too simplistic to provide a deeper insight into solvational mechanisms controlling aggregation over a broad range of cosolvent concentrations. In water/ethanol mixtures, the concentration of alcohol has nonmonotonic effects on the physicochemical properties of the system, which is manifested, for instance, in the biphasic dependencies of compressibility, etc. (*42*). In diluted ethanol, its molecules are singly dispersed. However, clustering of the organic solvent is favored with its growing share in the mixture with water. The changing molecular organization of the liquid (single EtOH molecules in water → ethanol clusters → single water molecules in ethanol) correlates not only with macroscopic physical parameters of the water/ethanol system but also with trends of thermodynamic stability of dissolved proteins. EtOH molecules are singly dispersed up to 0.06 molar fraction and then begin to cluster, which coincides with a reversal of growth trends of ΔH_{unf} and ΔS_{unf} of lysozyme in a H_2O/EtOH system (*42*, *43*). In the language of solvational thermodynamics, ethanol is preferentially excluded at low and preferentially bound at high concentrations, therefore most likely acting as a stabilizer in the former case and as a denaturant in the latter (*11*). Interestingly, the stabilizing effect of osmolytes may further accelerate the aggregation process. This follows form the fact that stabilizers (kosmotropes, osmolytes, and "chemical chaperones") do not promote folding per se but, through the preferential hydration, reduce the level of exposure of protein solvophobic groups, which is achieved either in the native state (folding) or in the amyloid state (aggregation). In that context, there is no contradiction in a cosolvent or cosolute promoting protein self-assembly, and still behaving as an osmolyte (*12*).

The PPC data obtained in the presence of EtOH (Figure 5B) are puzzling since a positive slope of an $\alpha_P - T$ curve is expected only for hydrophobic solutes (*30*), quite the opposite of that for folded globular proteins. This suggests direct binding of ethanol to the protein taking place, rendering the protein−water interface markedly more hydrophobic. The direct insulin−HAc interactions, yielding an analogous shape of the $\alpha_P - T$ plot, have been reported (*25*).

The intricate nature of the ethanol-induced perturbations of insulin aggregation involves its accelerating destabilization and monomerization of native molecules, promoting less structured aggregates, and, finally, slowing the aggregation at the highest alcohol concentrations (Figure 4B). The latter is presumably due to strong electrostatic repulsions between charged monomers when the dielectric constant of the solvent and hence Debye screening decrease. In the low-concentration range, EtOH appears to tune the amyloidal stacking through preferential hydration and only partial binding to the protein. In Figure 8, a conventional illustration of the preferential hydration concept, according to ref *11*, is juxtaposed with the case of self-assembling amyloid, wherein thermodynamic costs of exposure of solvophobic groups are controlled by osmolytes and denaturants. We propose that in a fibrillar self-assembling system, alignment of neighboring β-strands (Figure 8B), weakening the unfavorable protein−solvent interactions in amyloid (e.g., through clustering of hydrophobic side chains), is an equivalent of the burial-through-folding in single-protein molecules (Figure 8A). Such a scenario is consistent with amyloid structural models based on either the β-helix (*44*) or the "stacked β-rings" motif (*20*). According to this hypothesis, solvational interactions at the early stage of formation of aggregation nuclei (template) are critical for selection of thermodynamically favorable alignment modes. Fibrils representing self-assembly according to different modes are expected to vary in stability because of different packing and solvation of side chains, which can be a decisive factor controlling conformational transitions (*45*), and different energies of interstrand hydrogen bonding. This explains the different energies of interstrand hydrogen bonding visible in the FT-IR spectra of insulin amyloids (Figure 3D). A favorably hydrated assembly may be preferred at the expense of a more strained (but not necessarily frustrated) hydrogen bonding pattern. The strongest hydrogen bonding has been detected in the aggregates prepared in the presence of ethanol concentrations exceeding 20 wt % (Figure 3E), i.e., when the cost of exposure of hydrophobic residues is lowest and amorphous aggregates replace fibrils (Figure 6).

Configurational consequences of the proposed "hydrational bias" toward selection of a particular strand-to-strand alignment mode are expected to reach beyond hydrogen bonding patterns. Figure 8B shows schematically that orderly clustering of hydrophilic and hydrophobic side chains alongside the protofilaments may, through a motif repetition, create "ridges" and "groves", marked as blue and red lines, respectively. Such organization of hydrophobic groups could

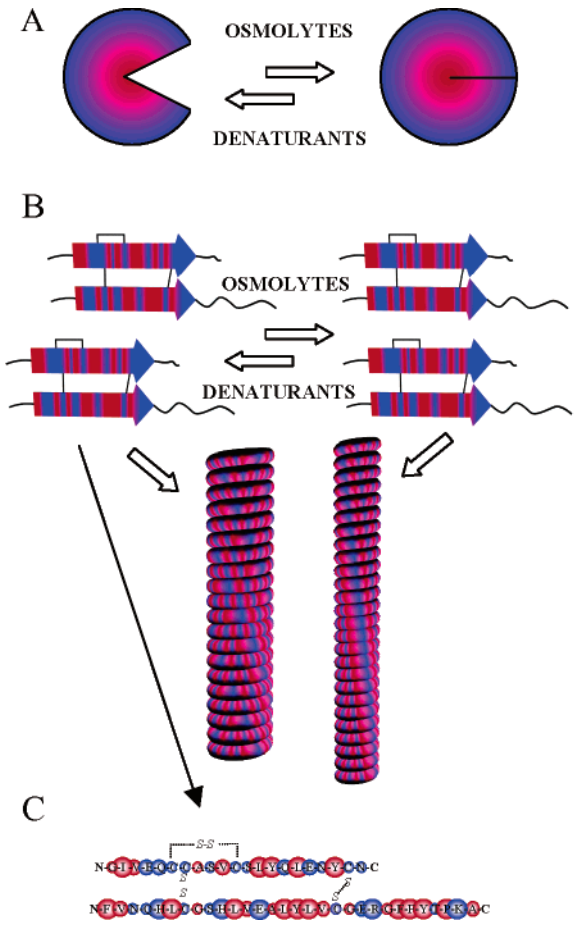

FIGURE 8: Schematic representation of the hypothetical solvational mechanism of inducing distinct amyloid types in a single protein species. Osmolytes and denaturants influence protein hydration, and the thermodynamic bias toward the exposure of the interior, which may disfavor or favor unfolding of the protein [(A) after Timasheff (*11*), where hydrophobic elements are red and hydrophilic elements blue]. (B) Different alignments of neighboring β-strands within an amyloid protofilament may permit surface clustering of hydrophobic residues and effectively reduce the number of unfavorable contacts with water. The thermodynamic costs associated with distinct alignment modes will be affected by the presence of osmolytes and denaturants favoring one assembly mode over another. (C) Bovine insulin sequence with superimposed relative volumes and hydrophobic properties of the amino acid side chain residues.

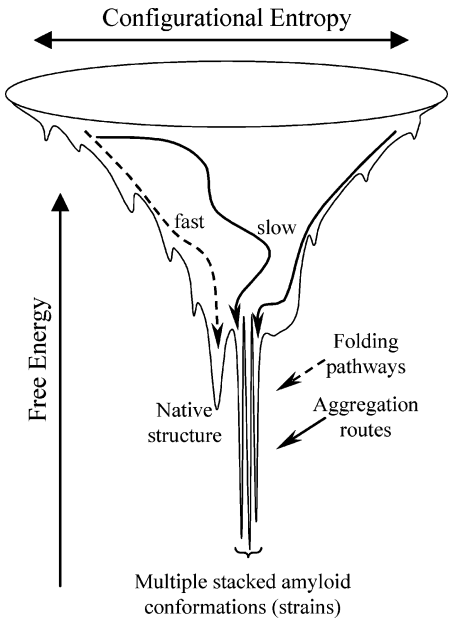

FIGURE 9: Amyloid strains and a folding funnel model for *n* protein molecules. High-energy/high-entropy unfolded states are competent to step on either folding (dashed) or aggregation (solid) routes. The shape of the folding funnel warrants that under physiological conditions, conformations surf fast downward, reaching the native state. Prolonged destabilization of the native conformation and high protein concentrations enhance the probability of nucleation and autocatalytic aggregation, i.e., entering an aggregation pathway. Aggregation is expected to reduce the global free energy beyond the native state level. Amyloids are highly ordered periodic structures, leaving negligible motional freedom to the polypeptide chain and thus reducing the conformational entropy. The cooperative character of fibril assembly (for the *n* protein molecules involved) creates enormous energy barriers for any interstrain transition, which in the end renders the energy landscape comblike-shaped.

become a driving force for intertwining protofilaments in the hierarchical formation of mature amyloid. The varying ThT and ANS binding properties of fibrils grown in different cosolvents may just correspond to such different "lateral" hydrophobicities of fibrils (Figure 7).

The patterns of amyloidogenic self-assembly are vulnerable to subtle hydrational effects mostly in the nucleation phase. Once the fibrillar template is formed, incoming protein monomers face just one predetermined option of packing and adapting to the seed conformation. The template-assisted formation of amyloid is fast and kinetically controlled, and therefore more likely to produce fibrils with the initial template conformation than a conformation otherwise spontaneously formed under particular solvational conditions. The conformational polymorphism and the autocatalytic character of aggregation may be the essential conditions leading to amyloid "strains", whose well-known medical and molecular aspects have been in the focus of the prion research (*29*). Different solvational conditions encountered by proteins destabilized in vivo (e.g., via natural osmolytes and vicinities of cellular membranes) could provide the physicochemical basis for multiple strains (*20*, *46*, *47*). Recently, we have reported the strainlike behavior of the two types of insulin amyloid formed in the presence and absence of ethanol (*27*, *28*). Because insulin is a protein genetically distant from prions, it suggests that the prion strains themselves may reflect a common, generic feature of amyloids. This prompts curiosity about how the putative prevalence of amyloid strains in different proteins should "update" a general protein energy landscape. Since protein aggregation appears to bring protein molecules to an energy minimum deeper than the native conformation level (*48*), this has called for revising the standard funnel model (*49*, *50*). The energy landscape shown in Figure 9 has the amyloid minimum comblike-shaped, spread into narrow competitive minima separated by enormous energy barriers. This is reminiscent of "weeping willow" landscape patterns (*51*). High-energy barriers facing interstrain transitions may be overcome only by a collective disassembly of the fibril.

In conclusion, we have shown that aggregation of insulin may be controlled by the presence of ethanol at several stages of this hierarchical process. The hydrational state of the protein, especially in the nucleation phase of aggregation, has profound consequences for its self-assembling pattern, and may be among decisive factors determining the physicochemical and biological properties of the mature amyloid. We have proposed a solvational mechanism of induction of

amyloid strains in insulin, which may be useful as a model tool in further studies of the molecular basis of polymorphism of non-native protein assemblies.

REFERENCES

1. Dobson, C. M. (1999) Protein misfolding, evolution and disease, *Trends Biochem. Sci. 24*, 329−332.
2. Fandrich, M., Fletcher, M. A., and Dobson, C. M. (2001) Amyloid fibrils from muscle myoglobin: Even an ordinary globular protein can assume a rogue guise if conditions are right, *Nature 410*, 165−166.
3. Nielsen, L., Khurana, R., Coats, A., Frokjaer, S., Brange, J., Vyas, S., Uversky, V. N., and Fink, A. L. (2001) Effect of environmental factors on the kinetics of insulin fibril formation: Elucidation of the molecular mechanism, *Biochemistry 40*, 6036−6046.
4. Ahmad, A., Millett, I. S., Doniach, S., Uversky, V. N., and Fink, A. L. (2003) Partially folded intermediates in insulin fibrillation *Biochemistry 42*, 11404−11416.
5. Ahmad, A., Millett, I. S., Doniach, S., Uversky, V. N., and Fink, A. L. (2004) Stimulation of insulin fibrillation by urea-induced intermediates, *J. Biol. Chem. 279*, 14999−15013.
6. Sluzky, V., Tamada, J. A., Klibanov, A. M., and Langer, R. (1991) Kinetics of Insulin Aggregation in Aqueous Solutions upon Agitation in the Presence of Hydrophobic Surfaces, *Proc. Natl. Acad. Sci. U.S.A. 88*, 9377−9381.
7. Munishkina, L. A., Phelan, C., Uversky, V. N., and Fink, A. L. (2003) Conformational behavior and aggregation of α-synuclein in organic solvents: Modeling the effects of membranes, *Biochemistry 42*, 2720−2730.
8. Munishkina, L. A., Henriques, J., Uversky, V. N., and Fink, A. L. (2004) Role of protein-water interactions and electrostatics in α-synuclein fibril formation, *Biochemistry 43*, 3289−3300.
9. Thirumalai, D., Klimov, D. K., and Dima, R. I. (2003) Emerging ideas on the molecular basis of protein and peptide aggregation, *Curr. Opin. Struct. Biol. 13*, 146−159.
10. Qu, Y. X., Bolen, C. L., and Bolen, D. W. (1998) Osmolyte-driven contraction of a random coil protein, *Proc. Natl. Acad. Sci. U.S.A. 95*, 9268−9273.
11. Timasheff, S. N. (2002) Protein-solvent preferential interactions, protein hydration, and the modulation of biochemical reactions by solvent components, *Proc. Natl. Acad. Sci. U.S.A. 99*, 9721−9726.
12. Yang, D. S., Yip, C. M., Huang, T. H. J., Chakrabartty, A., and Fraser, P. E. (1999) Manipulating the amyloid-β aggregation pathway with chemical chaperones, *J. Biol. Chem. 274*, 32970−32974.
13. Liu, D. F., Wyttenbach, T., Carpenter, C. J., and Bowers, M. T. (2004) Investigation of noncovalent interactions in deprotonated peptides: Structural and energetic competition between aggregation and hydration, *J. Am. Chem. Soc. 126*, 3261−3270.
14. Whittingham, J. L., Scott, D. J., Chance, K., Wilson, A., Finch, J., Brange, J., and Dodson, G. G. (2002) Insulin at pH 2: Structural analysis of the conditions promoting insulin fibre formation, *J. Mol. Biol. 318*, 479−490.
15. Brems, D. N., Brown, P. L., Heckenlaible, L. A., and Frank, B. H. (1990) Equilibrium denaturation of insulin and proinsulin, *Biochemistry 29*, 9289−9293.
16. Millican, R. L., and Brems, D. N. (1994) Equilibrium intermediates in the denaturation of human insulin and two monomeric insulin analogs, *Biochemistry 33*, 1116−1124.
17. Hua, Q. X., and Weiss, M. A. (2004) Mechanism of insulin fibrillation: The structure of insulin under amyloidogenic conditions resembles a protein-folding intermediate, *J. Biol. Chem. 279*, 21449−21460.
18. Dzwolak, W., Ravindra, R., Lendermann, J., and Winter, R. (2003) Aggregation of bovine insulin probed by DSC/PPC calorimetry and FTIR spectroscopy, *Biochemistry 42*, 11347−11355.
19. Bouchard, M., Zurdo, J., Nettleton, E. J., Dobson, C. M., and Robinson, C. V. (2000) Formation of insulin amyloid fibrils followed by FTIR simultaneously with CD and electron microscopy, *Protein Sci. 9*, 1960−1967.
20. Jimenez, J. L., Nettleton, E. J., Bouchard, M., Robinson, C. V., Dobson, C. M., and Saibil, H. R. (2002) The protofilament structure of insulin amyloid fibrils, *Proc. Natl. Acad. Sci. U.S.A. 99*, 9196−9201.
21. Khurana, R., Ionescu-Zanetti, C., Pope, M., Li, J., Nielsen, L., Ramirez-Alvarado, M., Regan, L., Fink, A. L., and Carter, C. A. (2003) A general model for amyloid fibril assembly based on morphological studies using atomic force microscopy, *Biophys. J. 85*, 1135−1144.
22. Jansen, R., Grudzielanek, S., Dzwolak, W., and Winter, R. (2004) High pressure promotes circularly shaped insulin amyloid, *J. Mol. Biol. 338*, 203−206.
23. Jansen, R., Dzwolak, W., and Winter, R. (2005) Amyloidogenic Self-Assembly of Insulin Aggregates Probed by High Resolution Atomic Force Microscopy, *Biophys. J. 88*, 1344−1353.
24. Nielsen, L., Frokjaer, S., Carpenter, J. F., and Brange, J. (2001) Studies of the structure of insulin fibrils by Fourier transform infrared (FTIR) spectroscopy and electron microscopy, *J. Pharm. Sci. 90*, 29−37.
25. Dzwolak, W., Ravindra, R., and Winter, R. (2004) Hydration and structure: The two sides of the insulin aggregation process, *Phys. Chem. Chem. Phys. 6*, 1938−1943.
26. Nichols, M. R., Moss, M. A., Reed, D. K., Cratic-McDaniel, S., Hoh, J. H., and Rosenberry, T. L. (2005) Amyloid-β protofibrils differ from amyloid-β aggregates induced in dilute hexafluoroisopropanol in stability and morphology, *J. Biol. Chem. 280*, 2471−2480.
27. Dzwolak, W., Smirnovas, V., Jansen, R., and Winter, R. (2004) Insulin forms amyloid in a strain-dependent manner: An FT-IR spectroscopic study, *Protein Sci. 13*, 1927−1932.
28. Dzwolak, W., Jansen, R., Smirnovas, V., Loksztejn, A., Porowski, S., and Winter, R. (2005) Template-controlled conformational patterns of insulin fibrillar self-assembly reflect history of solvation of the amyloid nuclei, *Phys. Chem. Chem. Phys. 7*, 1349−1351.
29. Chien, P., Weissman, J. S., and DePace, A. H. (2004) Emerging principles of conformation based prion inheritance, *Annu. Rev. Biochem. 73*, 617−656.
30. Lin, L. N., Brandts, J. F., Brandts, J. M., and Plotnikov, V. (2002) Determination of the volumetric properties of proteins and other solutes using pressure perturbation calorimetry, *Anal. Biochem. 302*, 144−160.
31. Cordeiro, Y., Kraineva, J., Ravindra, R., Lima, L. M. T. R., Gomes, M. P. B., Foguel, D., Winter, R., and Silva, J. L. (2004) Hydration and packing effects on prion folding and β-sheet conversion: High pressure spectroscopy and pressure perturbation calorimetry studies, *J. Biol. Chem. 279*, 32354−32359.
32. Ravindra, R., Shuang, Z., Gies, H., and Winter, R. (2004) Protein encapsulation in mesoporous silicate: The effects of confinement on protein stability, hydration, and volumetric properties, *J. Am. Chem. Soc. 126*, 12224−12225.
33. Batchelor, J. D., Olteanu, A., Tripathy, A., and Pielak, G. J. (2004) Impact of protein denaturants and stabilizers on water structure, *J. Am. Chem. Soc. 126*, 1958−1961.
34. Brinkley, M. (1992) A brief survey of methods for preparing protein conjugates with dyes, haptens, and cross-linking reagents, *Bioconjugate Chem. 3*, 2−13.
35. Lakowicz, J. R. (1999) *Principles of Fluorescence Spectroscopy*, 2nd ed., Kluwer Academic/Plenum Publishers, New York.
36. Rusinova, E., Tretyachenko-Ladokhina, V., Vele, O. E., Senear, D. F., and Ross, J. B. A. (2002) Alexa and Oregon Green dyes as fluorescence anisotropy probes for measuring protein-protein and protein-nucleic acid interactions, *Anal. Biochem. 308*, 18−25.
37. Bartels, J., Tenbruggencate, P., Hellwege, K. H., Schäfer, K., and Schmidt Landoldt-Börnstein, E. (1955) *Zahlenwerke und Funktionen aus Physik, Chemie, Astronomie, Geophysik und Technik*, 6th ed., Vol. IV, Part 1, Springer-Verlag, Berlin.
38. Nielsen, L., Frokjaer, S., Brange, J., Uversky, V. N., and Fink, A. L. (2001) Probing the mechanism of insulin fibril formation with insulin mutants, *Biochemistry 40*, 8397−8409.
39. Barth, A. (2000) The infrared absorption of amino acid side chains, *Prog. Biophys. Mol. Biol. 74*, 141−173.
40. Smith, G. D., Duax, W. L., Dodson, E. J., Dodson, G. G., De Graaf, R. A. G., and Reynolds, C. D. (1982) The Structure of Des-Phe B1 Bovine Insulin, *Acta Crystallogr. B38*, 3028.
41. Chen, Y., and Wallace, B. A. (1997) Solvent effects on the conformation and far UV CD spectra of gramicidin, *Biopolymers 42*, 771−781.
42. Cinelli, S., Onori, G., and Santucci, A. (1997) Effect of aqueous alcohol solutions on the thermal transition of lysozyme: A calorimetric study, *J. Phys. Chem. B 101*, 8029−8034.
43. Calandrini, V., Onori, G., and Santucci, A. (2001) Examination by dynamic light scattering of lysozyme in water/alcohol mixtures, *J. Mol. Struct. 565*, 183−188.

44. Wetzel, R. (2002) Ideas of order for amyloid fibril structure, *Structure 10*, 1031−1036.
45. Dzwolak, W., Ravindra, R., Nicolini, C., Jansen, R., and Winter, R. (2004) The diastereomeric assembly of polylysine is the low-volume pathway for preferential formation of *β*-sheet aggregates, *J. Am. Chem. Soc. 126*, 3762−3768.
46. Prusiner, S. B. (1998) Prions, *Proc. Natl. Acad. Sci. U.S.A. 95*, 13363−13383.
47. Chien, P., and Weissman, J. S. (2001) Conformational diversity in a yeast prion dictates its seeding specificity, *Nature 410*, 223−227.
48. Gazit, E. (2002) The "Correctly folded" state of proteins: Is it a metastable state? *Angew. Chem., Int. Ed. 41*, 257−259.
49. Onuchic, J. N., and Wolynes, P. G. (2004) Theory of protein folding, *Curr. Opin. Struct. Biol. 14*, 70−75.
50. Dobson, C. M. (2004) Principles of protein folding, misfolding and aggregation, *Semin. Cell Dev. Biol. 15*, 3−16.
51. Wales, D. J., Miller, M. A., and Walsh, T. R. (1998) Archetypal energy landscapes, *Nature 394*, 758−760.

BI050281T